Planning for the Change: Mapping Sea Level Rise and Storm Inundation in Sherman Island Using 3Di Hydrodynamic Model and LiDAR

Yang Ju, Wei-Chen Hsu, John D. Radke, William Fourt, Wei Lang, Olivier Hoes, Howard Foster, Gregory S. Biging, Martine Schmidt-Poolman, Rosanna Neuhausler, Amna Alruheil, and William Maier

Abstract In California, one of the greatest concerns of global climate change is sea level rise (SLR) associated with extreme storm events. Several studies were conducted to statically map SLR and storm inundation, while its dynamic was

The original version of this book was revised. An erratum to the book can be found at DOI: 10.1007/978-3-319-40902-3_30

Y. Ju (✉) • W.-C. Hsu • W. Fourt • A. Alruheil
Department of Landscape Architecture and Environmental Planning, University of California, Berkeley, CA 94720-1820, USA
e-mail: yangju90@berkeley.edu

J.D. Radke
Department of Landscape Architecture and Environmental Planning, University of California, Berkeley, CA 94720-1820, USA

Department of City and Regional Planning, University of California, Berkeley, CA 94720-1820, USA

W. Lang
Department of Building and Real Estate, The Hong Kong Polytechnic University, Hung Hom, Kowloon, Hong Kong, China

O. Hoes
Faculty of Civil Engineering and Geosciences, Delft University of Technology, Stevinweg 1, 2628 CN, Delft, Netherlands

H. Foster • M. Schmidt-Poolman
The Center for Catastrophic Risk Management, University of California, Berkeley, CA 94720, USA

G.S. Biging • W. Maier
Department of Environmental Science, Policy, and Management, University of California, Berkeley, CA 94720, USA

R. Neuhausler
Department of City and Regional Planning, University of California, Berkeley, CA 94720-1820, USA

Department of Environmental Science, Policy, and Management, University of California, Berkeley, CA 94720, USA

P. Thakuriah et al. (eds.), *Seeing Cities Through Big Data*, Springer Geography, DOI 10.1007/978-3-319-40902-3_18

less studied. This study argues it is important to conduct dynamic simulation with high resolution data, and employs a 3Di hydrodynamic model to simulate the inundation of Sherman Island, California. The big data, high resolution digital surface model (DSM) from Light Detection and Ranging (LiDAR), was used to model the ground surface. The results include a series of simulated inundation, which show that when the sea level rises more than 1 m, there are major impacts on Sherman Island. In all, this study serves as a fine database for better planning, management, and governance to understand future scenarios.

Keywords Sea level rise • Mapping • 3Di hydrodynamic model • LiDAR • Sherman island

1 Introduction

In California's coastal areas, one of the great concerns of global climate change is sea level rise (SLR) associated with extreme high tides (Heberger et al. 2009). By 2100, mean sea level (MSL) will rise between 1.2 and 1.6 m (Bromirski et al. 2012), and this will cause a series of impacts along coastal areas, such as inundation and flooding of coastal land, salt water intrusion, increased erosion, and the decline of coastal wetlands, etc. (Nicholls and Cazenave 2010; Titus et al. 1991). Among all the impacts, flood risk is likely the most immediate concern for coastal regions.

This threat can be more severe in the Sacramento-San Joaquin Delta (the Delta), as many of its islands are 3–8 m below sea level (Ingebritsen et al. 2000). These islands are protected by more than 1700 km of levees (Mount and Twiss 2005), with standard cross sections at a height of 0.3 m above the estimated 100-year flood elevation (Ingebritsen et al. 2000). However, with a projected SLR between 1.2 and 1.6 m, these current levees can be easily overtopped, and the islands can be flooded.

Several efforts were made in the adjacent San Francisco Bay area (the Bay Area) to measure and understand the impact of SLR and storm inundation (Biging et al. 2012; Heberger et al. 2009; Knowles 2009, 2010). By using computer models, these studies intersected a water surface with a ground surface to identify inundated areas. The water surface could be interpolated from measured water level data at existing gauges (Biging et al. 2012), while the ground surface was usually obtained from LiDAR that provided fine resolution from 1 to 5 m. It should be noted that the interpolated water surface is static since it only describes the water surface condition at a particular water level, such as MSL or mean higher high water (MHHW) level. However, real tides and storm events are dynamic processes. The Bay Area and the Delta are characterized by semi-diurnal tides each day, meaning there are two uneven heights of high tide and low tide, and should be modeled dynamically to simulate all stages in the tidal cycle and the movements of tides during a storm event.

Therefore, a 3Di hydrodynamic model (Stelling 2012), was used in this study to better simulate the dynamics of tidal interaction during an extreme storm event. In addition, a 1 m resolution digital surface model (DSM) was generated from LiDAR in order to accurately describe the ground surface and to indicate the water flow

pathway for 3Di simulations. A near 100-year storm with various scenarios of SLR was simulated in the Delta's Sherman Island, where significant critical infrastructure existed. Inundation extent, frequency, and average depth were mapped and analyzed based on the model outputs. Finally, a spatial resolution sensitivity analysis of DSM was conducted. Through this entire exercise, this study hopes to build a fine database for better planning, management, and governance to understand future scenarios.

2 Study Area

The study area, Sherman Island and its adjacent regions, is located at the confluence of Sacramento River and San Joaquin River (Fig. 1). Sherman Island is one of the major islands in the Delta, and is located at the transition from an estuarine system

Fig. 1 Map of study area, Sherman Island

to a freshwater system. This island has significant infrastructure, including Highway 160, electric high-power transmission lines and natural gas pipelines. It is also the place where the infrastructure passes the Delta from north to south. According to NOAA, MSL (1983–2001 epoch) measured at a nearby NOAA Port Chicago Gauge is 1.116 m, and MHHW (1983–2001 epoch) is 1.833 m (NOAA Tide and Currents 2010), based on North American Vertical Datum of 1988 (NAVD 88), a commonly used datum in North America for vertical survey. The average elevation of Sherman Island is below MSL. Therefore the island is surrounded by extensive levees to protect it from inundation. Even with this levee system, the island still suffered from flooding due to levee failures. For example, the most recent levee failure and flooding in 1969 costed the Army Corps of Engineers approximately $600,000 for repairing, resloping, and regrading the levee break area (Hanson 2009). Even without a levee failure, the island is still at risk in the face of SLR. The lowest point of the levees in the study area is 2.11 m above NAVD 88. If the SLR by year 2100 is 1.4 m, then the MSL will rise to 2.25 m and the levees in the study area will be easily overtopped and the entire Sherman Island will be flooded. Considering the importance of Sherman Island's infrastructure and its potential exposure to SLR, it is a critical region and needs to be studied.

3 Data and Methods

3.1 Overview

To understand the impact of SLR inundation, a water surface and a ground surface are required to identify the spatial extent of inundated areas. A hydrodynamic model, 3Di (Stelling 2012), was employed in this study to simulate the water surface from a 72-h, near 100-year storm associated with 0, 0.5, 1.0, 1.41 m SLR scenarios. The ground surface, or a DSM, was generated from airborne LiDAR to capture the terrain and important ground objects, e.g. levees. The model output is a time-series of inundations, providing spatial extent, inundation depth, and water level. The workflow is shown in Fig. 2. All elevation data use NAVD 88.

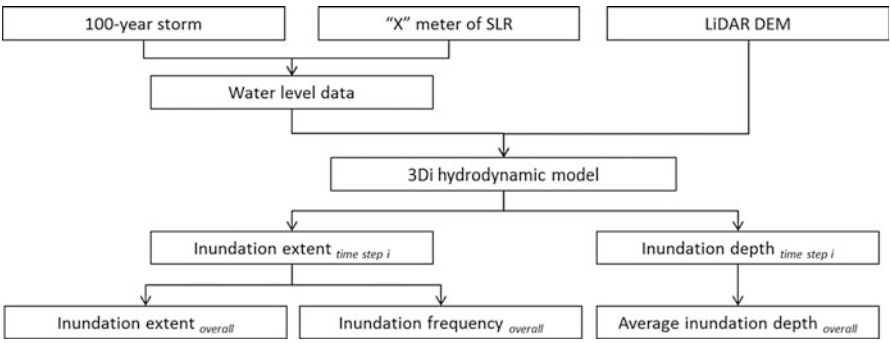

Fig. 2 Work flow of this study

3.2 3Di Hydrodynamic Model

The 3Di hydrodynamic model (Stelling 2012), developed by TU-Delft, Netherlands, dynamically simulates the movement of water through a digital ground surface. It employs an advanced approach for flooding simulation, allowing higher resolution and faster speed compared to existing hydrodynamic models (Van Leeuwen and Schuurmans 2012). The model is unique as it combines four specific methods: a sub-grid method where fine grids are clustered into coarser grids to calculate water levels and velocities (Dahm et al. 2014), a quadtree method which hierarchically decomposes the ground surface into a coarse grid and reduces the number of grid cells (Dahm et al. 2014), a bottom friction technique which accounts for the spatial variation of the roughness in the fine grid when calculating by coarse grid (Dahm et al. 2014; Stelling 2012), and a 'finite-volume staggered grid method for shallow water equations with rapidly varying flows, including semi-implicit time integration' (Stelling 2012).

The inputs of the model include time-series water level data and ground surface data. The output of the model is a time-series of simulated inundation that provides extent, depth, and water level. The time interval of the output is defined by the user. By further processing, the user can generate inundation frequency and average inundation depth by combining results from each time step. With an additional dimension of time, this model simulates the dynamics of flood and identifies the most exposed locations from SLR and storm inundation. In addition, with the time-series output, an inundation animation can be created to provide visual communication for the general public, making it a great educational tool.

3.3 Water Level Data

The first input of the 3Di model is water level data. To estimate the impact of a worst case scenario, a near 100-year storm event was used as the baseline, and SLR increments were added to the baseline. Being a dynamic model, 3Di requires time-series water level data for the entire storm event as input. However, existing 100-year storm calculation methods and studies (Zervas 2013) only provide estimates of water levels for a single stage such as MSL, MHHW, and mean lower low water (MLLW) level. Therefore, a historic storm whose peak water level was close to the 100-year storm was used as the water level input. Shown in Table 1, two storms that occurred in 1983 exceed the estimated 100-year storm at San Francisco NOAA tide station (NOAA ID: 9414290), and a third highest storm occurred on Feb. 6, 1998 that had a peak water level close to the estimated 100-year storm (Zervas 2013). All of these three extreme storms occurred during El Niño years.

Considering the storm's peak water level and availability of data, the Feb. 6, 1998 storm was selected as the storm to be simulated. More specifically, this study simulated this storm event over 72-h, from Feb 5 to Feb 7, 1998, to allow the

Table 1 Estimated and historic extreme storms at San Francisco and Port Chicago NOAA gauge

Station name	Date	Estimated 100-year storm (m)	Peak water level (m)
San Francisco	01/27/1983	2.64	2.707
	12/03/1983		2.674
	02/06/1998		2.587
Port Chicago	02/06/1998	Not available	2.729

model simulation to capture the complete storm movements through the study area. The water level data used for the 3Di simulation was retrieved from the nearby NOAA Port Chicago gauge (NOAA ID: 9415144), which provided measured water levels with 6-min intervals during the storm event.

As for the SLR scenarios, Cayan et al. (2009) and Cloern et al. (2011) studied the projected water level at Golden Gate in the Bay Area, and found that the time that sea levels exceed the 99.99th historical percentile of water elevation would increase to 15,000 h per decade by year 2100. And the 99.99th historical percentile is 1.41 m above year 2000's sea level. This study assumed that 1.41 m would be the maximum SLR by year 2100. This study also analyzed scenarios of 0, 0.5, and 1.0 m SLR to show how the impact changed with rising sea level. SLR was added on top of the baseline water level to simulate each scenario.

3.4 Ground Surface Data

The second input for the 3Di model is a fine spatial resolution DSM. The DSM was constructed based on LiDAR data, which used active remote sensing technology to measure the distance to target by illuminating the target with light pulses from a laser (Wehr and Lohr 1999). The density of the LiDAR data used in this study is 1 point per 0.7 m^2, and there are approximately 140 million points covering the study area. The DSM obtained from LiDAR in this study was originally 1 m resolution, and was resampled to 4 m resolution by the maximum aggregation method (ESRI 2015) to meet the computing limitations. In this method, a coarse grid cell obtains the maximum value of the fine grid cells in the coarse grid cell's spatial extent. Even though the DSM was aggregated to 4 m, this spatial resolution still accurately described the actual ground surface by precisely delineating objects such as levees, ditches, buildings, and the pathways that water moved through.

As aforementioned, the 3Di model has a limitation in the total number of grid cells that it can process, and it uses the quad-tree approach to reduce the total number of grid cells for model computation. The quad-tree is a data structure that is based on the regular decomposition of a square region into quadrants and sub-quadrants (Mark et al. 1989). 3Di draws finer quadrants/grid cells when elevation changes greatly within a short x, y distance, which then preserves detailed information while reducing the amount of data. Considering Sherman Island is

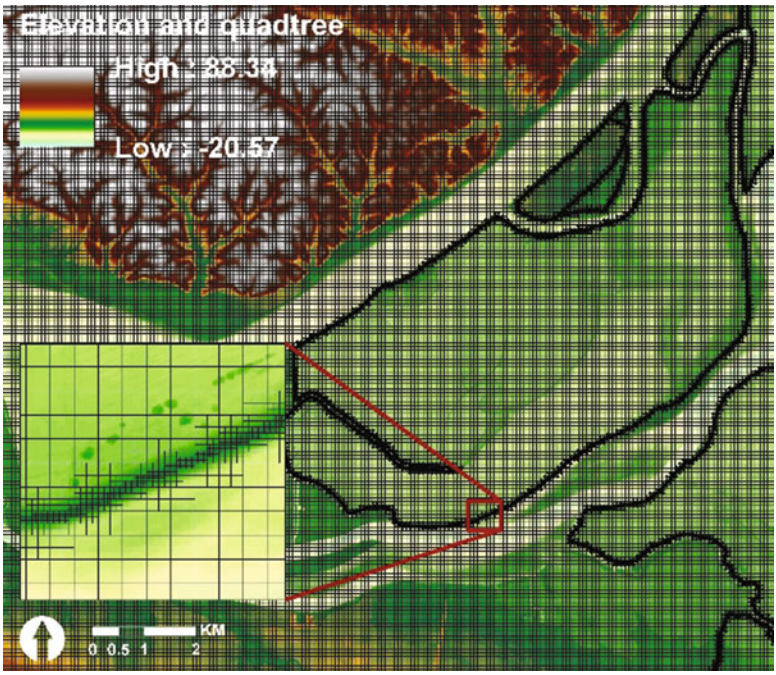

Fig. 3 DSM and guad-tree grid, which show 3Di draws finer grid cells along the levees and coarser grid cells for the other areas

relatively flat and the only abrupt change in topography is due to the levees, only levee data were used in the model to create finer grid cells, and coarser grid cells were generated for the rest of the study area that was more homogenous. The DSM and the quad-tree grid for Sherman Island are shown in Fig. 3.

4 Results

The 3Di simulation output is a time-series of inundated areas with an output time interval that is defined by the user. Each output provides the spatial extent and depth of inundation. In this study, the time interval was set as 1 h, and a total of 72 outputs were generated from the model. With the time-series outputs, this study analyzed inundation frequency and average inundation depth. Figure 4 shows the inundation extent and depth in hour 1, 24, 48, 72 for the simulated near 100-year storm associated with 0, 0.5, 1.0, and 1.41 m SLR.

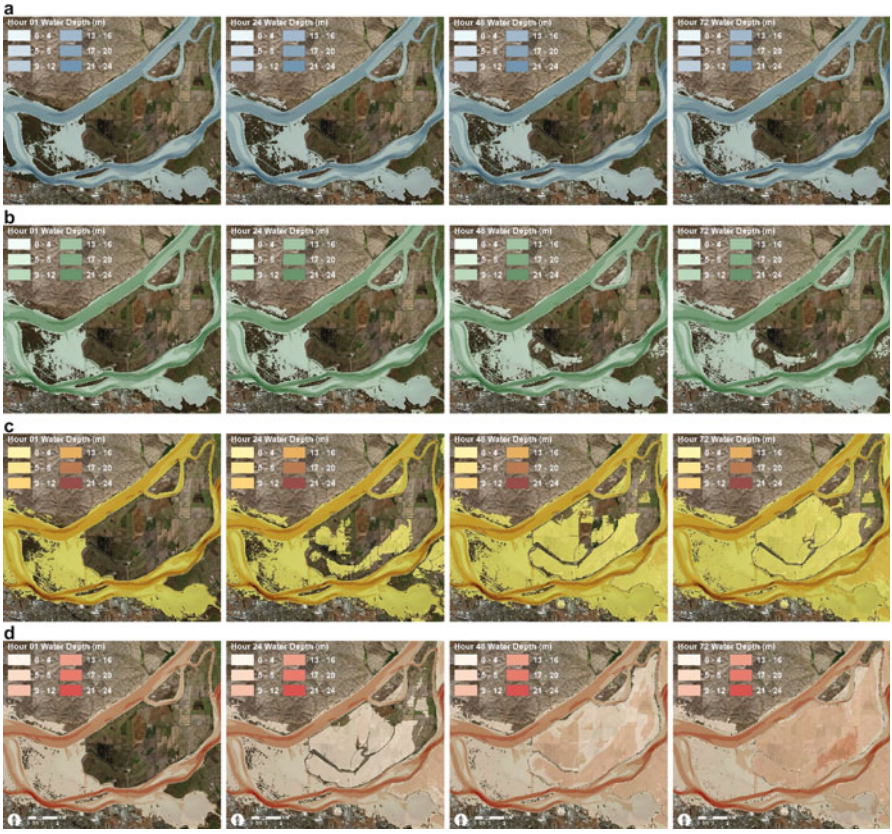

Fig. 4 Examples of simulated inundation from the 72-h, 100-year storm associated with 0 m (**a**), 0.5 m (**b**), 1.0 m (**c**), and 1.41 m (**d**) SLR, showing inudation extent and depth in hour 1, 24, 48, 72, respectively

4.1 Inundation Extent

The results show that during a 100-year storm, a total of 14.68 km^2 of land is inundated in the study area. With 0.5 m SLR, a total 20.67 km^2 of land is inundated, with 1.0 m SLR, a total of 57.87 km^2 of land is inundated, and with 1.41 m SLR, a total of 72.43 km^2 of land is inundated (Table 2). The inundation extent for different SLR scenarios is mapped in Fig. 5. The western end of Sherman Island is constantly underwater in all the modeled SLR scenarios as it is not protected by levees. In the 0.5 m SLR scenario, only minor inundation occurred in the rest of the island. In the 1.0 m SLR scenario, over half of the remaining Sherman Island is inundated and in the 1.41 m SLR scenario, the entire Sherman Island is inundated. This progress shows that when the sea level rises above 1.0 m, it will cause major flood impacts on Sherman Island.

Table 2 Statistical summary of inundation by a 100-year storm with different levels of SLR

SLR (m)	Inundated area (km^2)	Area by inundation frequency (km^2)			Area by average inundation depth (km^2)		
		Low (0.00–0.21)	Medium (0.22–0.64)	High (0.65–1.00)	Low (0.00–1.98 m)	Medium (1.99–4.01 m)	High (4.02–13.22 m)
0	14.68	4.40	4.99	5.30	14.64	0.04	0.00
0.5	20.67	3.26	7.33	10.08	20.51	0.15	0.00
1.0	57.87	6.82	23.93	27.11	49.55	8.31	0.01
1.41	72.43	2.37	15.52	54.54	23.91	32.67	15.86

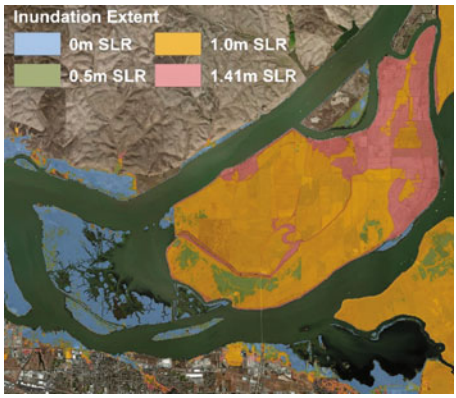

Fig. 5 Inundated area by a near 100-year storm associated with 0, 0.5, 1.0, 1.41 m SLR

4.2 Inundation Frequency

Storm is a dynamic process, and impacted areas are not permanently under water during the entire storm event. Thus, this study analyzed inundation frequency by using (1) and (2):

$$I_{x,y,i} = \begin{cases} 1, & \textit{inundated} \\ 0, & \textit{not inundated} \end{cases} \tag{1}$$

$$F_{x,y} = \frac{\sum_{i=1}^{n} I_{x,y,i}}{n} \tag{2}$$

where $I_{x,y,i}$ is whether grid cell in column x, row y gets inundated at hour i, $F_{x,y}$ is inundation frequency for grid cell in column x, row y, and n is total number of outputs, which equals 72 in this study since a 72-h event was simulated.

The inundation frequency calculated here is the proportion of hours each piece of land (i.e. a 4 m × 4 m grid cell) gets inundated in the entire 72-h storm event. This study then classified the inundation frequency in the 1.41 m SLR scenario using a natural breaks method, which minimizes the variance within classes and maximizes the variance between classes (ESRI 2015). From this classification, low frequency is 0.00–0.21, medium frequency is 0.22–0.64, and high frequency is 0.65–1.00. The results from other scenarios were classified using the 1.41 m SLR scenario's classification in order to compare between the scenarios. The inundation frequency is shown in Fig. 6 for the four scenarios, and a statistical summary is shown in Table 2. From the results, it is observed that when the sea level rises, low frequency areas decrease while high frequency areas increase, therefore showing that more land will be permanently inundated in the future with such rises.

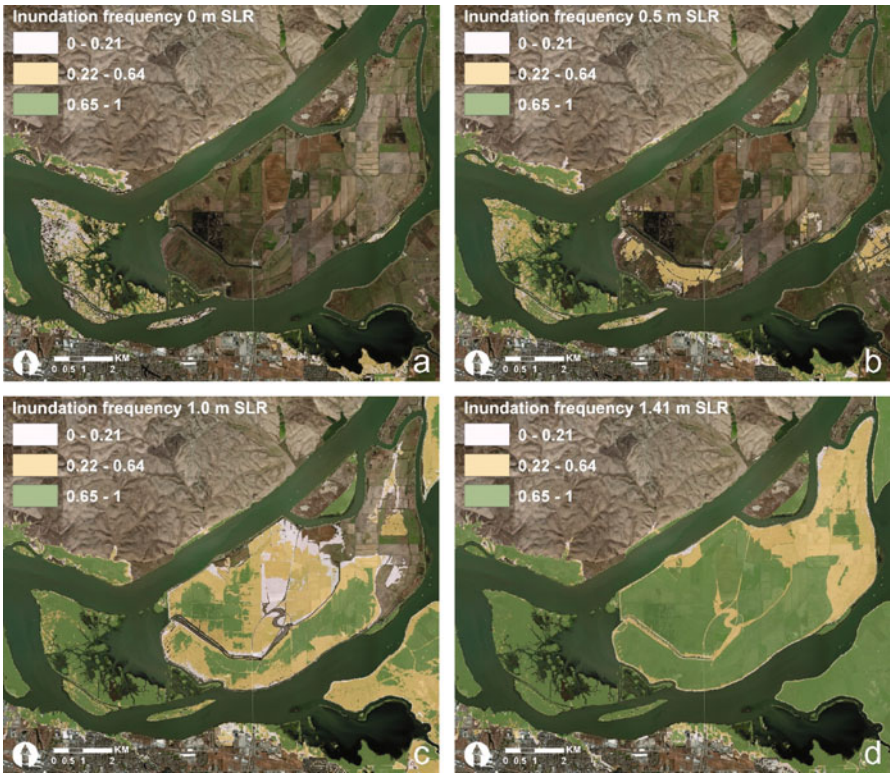

Fig. 6 Inundation frequency during the 3-day 100-year storm associated with 0 m (**a**), 0.5 m (**b**), 1.0 m (**c**), and 1.41 m (**d**) SLR

4.3 Average Inundation Depth

This study also analyzed average inundation depth, as the inundation depth on top of each piece of land varied in a storm event. Average inundation depth was calculated by (3):

$$D_{x,y} = \frac{\sum_{i=1}^{n} d_{x,y,i}}{n} \tag{3}$$

where $D_{x,y}$ is average inundation depth (m) at grid cell in column x, row y, $d_{x,y,\,i}$ is inundation depth at grid cell in column x, row y, at hour i, and n is total number of outputs, which equals 72 in this study.

Similarly, this study classified average inundation depth in the 1.41 m SLR scenario by the natural breaks method. From this classification, low depth is 0–1.98 m, medium depth is 1.99–4.01 m, and high depth is 4.02–13.22 m. The

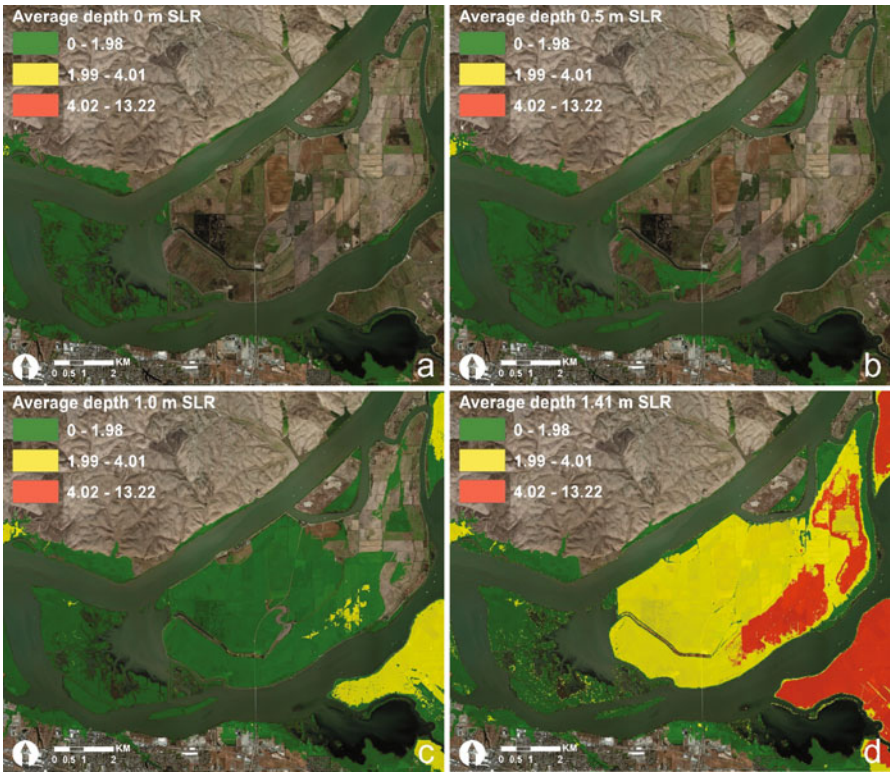

Fig. 7 Average inundation depth during the 3-day 100-year storm associated with 0 m (**a**), 0.5 m (**b**), 1.0 m (**c**), and 1.41 m (**d**) SLR

results from other scenarios were classified using the 1.41 m SLR scenario classification, in order to compare between the scenarios. The average inundation depth is shown in Fig. 7, and a statistical summary is shown in Table 2. The results show that in the 0.5 and 1.0 m SLR scenarios, the majority of inundated areas are under low inundation depth, and when it comes to the 1.41 m SLR, more areas are under medium and even high inundation depth.

4.4 DSM's Spatial Resolution Sensitivity Analysis

While 4 m resolution was used in the simulation as it was the finest resolution possible, it is important to test spatial resolution sensitivity of DSM and the effect on extent, frequency, and average depth. Surfaces with other resolution (5, 6, 10, 20, and 30 m) were used for the sensitivity analysis, while other model parameters remained the same. The same maximum aggregation method was

used here for generating those surfaces from the original, 1 m resolution surface, and the results from the 4 m simulation were used as the baseline for comparison. To quantify the sensitivity, percentage difference in area (4) was calculated for extent, and Root Mean Square Difference (RMSD) and Coefficient of Variation (CV) were calculated for depth and frequency (5) and (6). When calculating RMSD, coarse resolution's results were first resampled to 4 m resolution by the nearest neighbor method (ESRI 2015), and RMSD was calculated using the 4 m resolution grid cells.

$$Diff = \frac{A_i - A_4}{A_4} \times 100\% \tag{4}$$

where A_i is the inundated area with other resolution i (5, 6, 10, 20, and 30 m), A_4 is the inundated area with 4 m resolution.

$$RMSD = \sqrt{\frac{\sum_{t=1}^{n} (y_i - y_4)^2}{n}} \tag{5}$$

where y_i is a grid cell's value simulated with other resolution i, y_4 is the grid cell's value simulated with 4 m resolution, n is the total number of grid cells compared.

$$CV = \frac{RMSD}{\bar{y}_4} \tag{6}$$

where $\bar{y}_4$ is the mean value of grid cells simulated with 4 m resolution.

The analysis shows the model is sensitive to resolution (Tables 3, 4, and 5), emphasizing the importance for simulating with fine resolution data. Coarser spatial resolution data leads to greater differences compared to the baseline, as more low elevation areas are diminished by the maximum aggregation method, resulting in an more elevated ground surface, less inundated area, smaller inundation depth, and less frequent inundation. Furthermore, differences are generally greater in lower SLR scenarios (e.g. 0 and 0.5 m) than those in higher SLR scenarios (e.g. 1.0 and 1.41 m). This is because when sea level rises, those elevated areas due to aggregation start to be inundated, and their effect on the results starts to decrease.

Table 3 Percentage difference in inundated area under other resolutions

	Resolution (m)				
SLR (m)	5	6	10	20	30
0	2.51 %	5.25 %	11.46 %	23.19 %	31.24 %
0.5	2.15 %	3.67 %	9.43 %	21.60 %	30.10 %
1.0	0.36 %	−0.86 %	2.42 %	10.20 %	14.00 %
1.41	0.54 %	0.69 %	1.47 %	3.52 %	5.55 %

Table 4 RMSD and CV of average inundation depth under other resolutions

	SLR (m)	Resolution (m)					Mean depth (m) in 4 m simulation
		5	6	10	20	30	
RMSD	0	0.08	0.11	0.12	0.19	0.23	0.37
	0.5	0.11	0.12	0.16	0.25	0.30	0.50
	1	0.17	0.17	0.31	0.43	0.54	1.08
	1.41	0.22	0.26	0.32	0.48	0.80	2.80
CV	0	22.10 %	28.89 %	34.01 %	51.01 %	63.11 %	
	0.5	21.28 %	23.21 %	32.39 %	49.42 %	60.36 %	
	1	15.44 %	16.16 %	29.06 %	40.18 %	50.08 %	
	1.41	8.01 %	9.44 %	11.36 %	17.06 %	28.42 %	

Table 5 RMSD and CV of inundation frequency under other resolutions

	SLR (m)	Resolution (m)					Mean frequency in 4 m simulation
		5	6	10	20	30	
RMSD	0	0.12	0.13	0.20	0.28	0.32	0.05
	0.5	0.20	0.12	0.18	0.27	0.33	0.09
	1	0.07	0.08	0.12	0.19	0.23	0.24
	1.41	0.06	0.07	0.09	0.14	0.18	0.38
CV	0	238.33 %	264.60 %	395.08 %	560.44 %	654.42 %	
	0.5	222.09 %	133.04 %	203.42 %	303.57 %	363.82 %	
	1	30.29 %	33.10 %	49.24 %	76.42 %	92.92 %	
	1.41	15.21 %	17.31 %	23.81 %	36.10 %	46.19 %	

5 Discussion and Conclusions

5.1 Implication for Planning

This study creates a SLR and storm inundation dataset for Sherman Island and its adjacent areas. This is an important and initial step for policy makers, planners, and the public to understand the magnitude and spatial distribution of SLR and storm inundation. The big data, high resolution DSM, was used to accurately model the ground surface. The results show that with more than 0.5 m SLR, the levees protecting Sherman Island start to be overtopped. With 1.0 m SLR, nearly half of Sherman Island is inundated, and with 1.41 m SLR, the entire island is inundated. Based on this study, SLR impacts are significant, especially when SLR is greater than 1.0 m. Local governments can use the inundation water level to improve the levee system and construct new levees to protect areas with high inundation frequency. This dataset can also be employed in a suitability analysis for Sherman Island to identify areas with higher inundation risks, and to improve infrastructure planning and/or adopt different planning strategies for the rising sea level. Finally, the DSM's spatial resolution sensitivity analysis shows the importance of fine resolution data. Local governments should collect the best quality data possible to inform more accurate decision making.

Our future work further studies the SLR impacts on infrastructures, such as pipelines and roads. These infrastructures are designed to allow certain level of inundation, but this tolerance is limited. To better understand SLR and storm inundation impacts on these critical infrastructures, it is beneficial to know the duration and the depth of water sitting on top of any infrastructure. Static models have limitations as they only depict one stage of inundation, where the information on duration and flood dynamic is lost. The dynamic model implemented here provides the additional dimension of time. Subsequent studies can intersect the inundation dataset with infrastructure datasets to calculate the duration of impact, as well as the amount of water sitting on top of impacted infrastructure. To conclude, future researchers should identify when the infrastructure gets impacted, estimate the cost, and provide more detailed planning suggestions.

5.2 Limitations

This study has several limitations. First, the Sacramento-San Joaquin Delta region has a complex hydrologic system which is influenced by both the ocean and the rivers, making it difficult to conduct hydrologic modeling. Considering that Sherman Island is close to the mouth of the Delta, this study simplified the actual process and assumed that the island is only affected by tidal surges from the ocean. With the discharge from the Sacramento and San Joaquin River, the simulated process could be different. Second, the model did not incorporate other factors, such as subsidence, sediment deposition, wind, and rainfall. Being an "artificial" system, the Sacramento-San Joaquin Delta region has limited sedimentation and significant subsidence issues that would further exacerbate the impact of SLR inundation. As a result, the 3Di model might underestimate the SLR impacts on Sherman Island. Third, the water level data used in this study could be inaccurate, as there is no gauge currently available in the immediate region of the study area. Finally, the 3Di model has computing limitations that limit the number of grid cells processed to approximately 125,000 for each simulation. Our study lowered the DSM resolution, from the original 1 m resolution to 4 m, to accommodate the computing limitations. As a result, some topographic information, such as smaller ditches and roads, might not be reflected in the model.

5.3 Conclusions

No GIS model perfectly represents reality (Fazal 2008), and inundation models are usually a simple but effective method that identifies inundated areas (Tian et al. 2010). They provide the possibility to incorporate different datasets and generate models for planners, policy makers and the public to clearly see potential impacts. Compared to previous studies, our study provides a more detailed level of

information, and serves as a basis for future analysis in Sherman Island. We continues to generate similar datasets for the entire Bay and Delta, and intersect the datasets with objects of interest. With such efforts, we hope to get a better understanding about SLR, its impacts and possible countermeasures.

Acknowledgements This chapter was funded by the California Energy Commission – PIER, California Climate Change Impacts Program (UCB 500-11-016).

References

Biging GS, Radke JD, Lee JH (2012) Impacts of predicted sea-level rise and extreme storm events on the transportation in the San Francisco Bay Region. California Energy Commission, Sacramento

Bromirski PD et al (2012) Coastal flooding-potential projections 2000–2100. California Energy Commission, Sacramento

Cayan D et al (2009) Climate change scenarios and sea level rise estimates for the California 2008 Climate Change Scenarios Assessment. California Energy Commission, Sacramento

Cloern JE et al (2011) Projected evolution of California's San Francisco bay-delta-river system in a century of climate change. PLoS One 6(9):e24465

NOAA Tide and Currents (2010) Datums for 9415144, Port Chicago CA. http://tidesandcurrents.noaa.gov/datums.html?units=1&epoch=0&id=9415144&name=Port+Chicago&state=CA. Accessed 3 Aug 2015

Dahm R et al (2014) Next generation flood modelling using 3Di: a case study in Taiwan. In: DSD international conference 2014, sustainable stormwater and wastewater management, Hong Kong

ESRI (2015) Nearest neighbor resampling—GIS dictionary. http://support.esri.com/en/knowledgebase/GISDictionary/term/nearest%20neighbor%20resampling. Accessed 4 Aug 2015

Fazal S (2008) GIS basics. New Age International, New Delhi

Hanson JC (2009) Reclamation District 341, Sherman Island Five Year Plan 2009. http://ccrm.berkeley.edu/resin/pdfs_and_other_docs/background-lit/hanson_5yr-plan.pdf

Heberger M et al (2009) The impacts of sea-level rise on the California coast. California Energy Commission, Sacramento

Ingebritsen SE et al (2000) Delta subsidence in California; the sinking heart of the state. U.S. Geological Survey. http://pubs.usgs.gov/fs/2000/fs00500/. Accessed 3 Aug 2015

Knowles N (2009) Potential inundation due to rising sea levels in the San Francisco Bay Region. California Climate Change Center. http://www.energy.ca.gov/2009publications/CEC-500-2009-023/CEC-500-2009-023-D.PDF

Knowles N (2010) Potential inundation due to rising sea levels in the San Francisco Bay Region. San Francisco Estuar Watershed Sci 8(1). http://escholarship.org/uc/item/8ck5h3qn. Accessed 18 Dec 2014

Mark DM, Lauzon JP, Cebrian JA (1989) A review of quadtree-based strategies for interfacing coverage data with digital elevation models in grid form. Int J Geogr Inf Syst 3(1):3–14

Mount J, Twiss R (2005) Subsidence, sea level rise, and seismicity in the Sacramento–San Joaquin Delta. San Francisco Estuar Watershed Sci 3(1). http://escholarship.org/uc/item/4k44725p. Accessed 3 Sept 2014

Nicholls RJ, Cazenave A (2010) Sea-level rise and its impact on coastal zones. Science 328 (5985):1517–1520

Stelling GS (2012) Quadtree flood simulations with sub-grid digital elevation models. Proce ICE Water Manag 165(10):567–580

Tian B et al (2010) Forecasting the effects of sea-level rise at Chongming Dongtan Nature Reserve in the Yangtze Delta, Shanghai, China. Ecol Eng 36(10):1383–1388
Titus JG et al (1991) Greenhouse effect and sea level rise: the cost of holding back the sea. Coast Manag 19(2):171–204
Van Leeuwen E, Schuurmans W (2012) 10 questions to professor Guus Stelling about 3Di water managment. Hydrolink 3:80–82
Wehr A, Lohr U (1999) Airborne laser scanning—an introduction and overview. ISPRS J Photogramm Remote Sens 54(2–3):68–82
Zervas C (2013) Extreme water levels of the United States 1893–2010. Center for Operational Oceanographic Products and Services, National Ocean Service, National Oceanic and Atmospheric Administration